Journal Pre-proof

Design, fabrication, and characterization of a hydrostatic electroactive soft actuator for bio-inspired robots

Yiyuan Zhang, Haonan Zhang, Kuang Wang, Yuchen Liu, Yanru Mo, Li Wen

PII: S2667-3797(22)00037-7
DOI: https://doi.org/10.1016/j.birob.2022.100077
Reference: BIROB 100077

To appear in: *Biomimetic Intelligence and Robotics*

Received date : 12 September 2022
Revised date : 3 October 2022
Accepted date : 5 October 2022

Please cite this article as: Y. Zhang, H. Zhang, K. Wang et al., Design, fabrication, and characterization of a hydrostatic electroactive soft actuator for bio-inspired robots, *Biomimetic Intelligence and Robotics* (2022), doi: https://doi.org/10.1016/j.birob.2022.100077.

Design, fabrication, and characterization of a hydrostatic electroactive soft actuator for bio-inspired robots

Yiyuan Zhang[a,†], Haonan Zhang[a,†], Kuang Wang[a], Yuchen Liu[a], Yanru Mo[a], Li Wen[b,*]

[a] School of General Engineering, Beihang University, Beijing, China.
[b] School of Mechanical Engineering and Automation, Beihang University, Beijing, China.

* Corresponding author: liwen@buaa.edu.cn
† These authors contributed equally to this work.

ARTICLE INFO

Keywords: Transverse musculature, Constant-volume actuation, Laser processing, Dielectric actuator, Soft Robot

ABSTRACT

In this paper, we designed a hydrostatic electroactive soft actuator (HESA) inspired by octopus transverse musculature. We introduced the advantage of laser processing technology in HESA fabrication compared with existing similar actuators and discussed the effect of laser processing on the outer membrane of the actuator. In addition, a mathematical model was established for the single channel of the actuator, and the geometric parameters of the actuator were optimized by mathematical model simulation and experiments. We demonstrated the motion effect of the actuator. Our experiments show that the single piece of the actuator can achieve 32.2% strain in the axial direction and 7.8% strain in the radius direction. Furthermore, we stack three actuators together and describe their motion characteristics at different frequencies. The stacked actuators could realize axial elongation, radial shrinkage, and bend, which covers all the motion modes of the octopus biological transverse musculature. This study may lay a foundation for implementing the biomimetic soft actuator mimicking the octopus's transverse musculature, which is one less discussed but crucial muscular composition in the octopus-inspired arm research.

1. Introduction

Many soft-bodied animals in the natural world exhibit exciting mechanical and locomotor characteristics. The octopus uses their soft tentacles to grab distant objects [1,2] and complete complex movements. The elephant trunk can remove obstacles and suck water [3]. Geckos can use cilia on their palm to crawl on the wall [4]. These animals have evolved flexible physiological structures to adapt to the environment. Octopuses have been one of the most famous creatures in soft-bodied animals and inspired lots of soft robotics research [5–14]. Octopus has a highly flexible arm, which can accomplish highly elongating, bending, variable stiffness, and other behaviors. Such high movement flexibility can be attributed to its ingenious muscular hydrostats system [15].

A critical component of the octopus arm is the transverse musculature (as shown in blue in Fig. 1A), which moves under the constraint of constant volume: when actuated, it shrinkage in the radial direction and elongate in the axial direction at the same time. By actuating part of the transverse musculature, that part will elongate and cause a bending motion. When all parts of transverse musculature contract, the arm tends to elongate in the axial direction and contracts in the radius direction. A few forms of the octopus musculature-inspired robot have been developed before, the actuation including shape memory alloy (SMA) actuation [5,10], pneumatic actuation [9,14], and cable actuation [11,12]. Most of them could not show the radius shrinkage of the octopus arm, because they omit the transverse musculature due to its complex movement mode. Laschi *et al.* tried to mimic the transverse musculature [5,10,11,13]. However, a bio-inspired transverse musculature, which could achieve axial elongation, radial shrinkage, and bend, still lacks descriptions.

Similar to muscular hydrostats, the soft dielectric actuator is one kind of constant volume actuator. Based on dielectric elastomer (DE) actuators [16], Keplinger *et al.* added a high-voltage insulating oil layer between the elastomers of DE and proposed a self-healing hydraulic dielectric actuator (HASEL) [17]. It comprises three parts: elastic shell, high-voltage insulating oil, and flexible electrode. The composition allows the actuator to be equipped with hydraulic properties. The high-voltage insulating oil can protect the actuator to some extent in the case of high-voltage breakdown and improve the actuator's working duration. However, the common fabrication methods of HASEL actuators are relatively complex or tiring [17–19]. Keplinger *et al.*introduced a method of using a 3D printer as a CNC to process HASEL and a screen printing method for electrode fabrication, notably improving the efficiency of HASEL fabrication [20,21]. Nevertheless, the above fabrication methods still need to seal and cut the oil sac separately.

In this study, we designed a three-channel hydrostatic electroactive soft actuator based on the features of the transverse musculature. This actuator not only can bend but is also able to elongate in the longitudinal direction with a radius shrinkage (Fig. 1B).

This flexible actuator is filled with dielectric fluid so that it moves under volume constraints like muscular hydrostats. Based on the fabrication method of HASEL actuators, we fabricate HESA with laser processing instead of modifying a 3D printer to a CNC heat-sealing machine. The laser processing of HESA is an accurate fabrication method that combines the oil sac sealing and cut in one process run without any extra learning or modification of the laser processing system.

To deeper explore the HESA actuator, several geometry parameters are selected to optimize the longitudinal elongation capability. Then, the mathematical model was proposed, and the simulation was carried out. The performance of the laser sealing is tested by adjusting key processing parameters. Finally, we use the diving board to actuate the HESA to validate our designs.

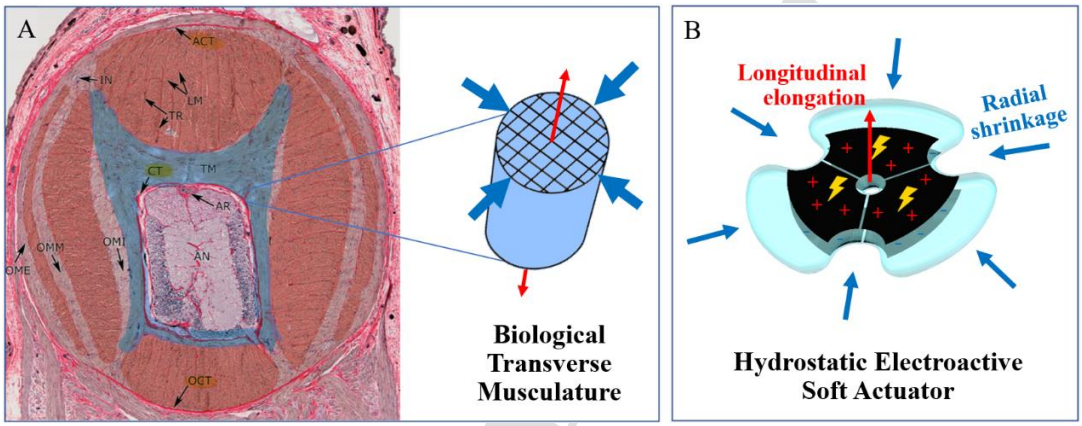

Fig. 1. An electroactive soft actuator inspired by the transverse musculature of muscular hydrostats. (**A**) Transverse musculature is a kind of muscular hydrostat that elongates axially and contracts in the radius direction under constant volume movement constraints. Adapted with permission. Copyright © 2007 Wiley-Liss, Inc. © 2012. Published by The Company of Biologists Ltd. (**B**) Model and the design of movements of biomimetic soft actuator HESA.

2. Method

2.1. The parametric design of HESA

In the muscular hydrostats system of the octopus, the structure of transverse musculature is similar to a four-point star; this kind of musculature arrangement enables the octopus arm to bend in 2 degrees of freedom. In our design of the HESA, the freedom of the biological octopus arm is guaranteed, and the complexity is reduced by simplifying the four-point star to a three-channel actuating system. The composition of HESA can be divided into three parts: flexible shell, dielectric oil, and flexible electrodes. In the fabrication process, we refer to the flexible shell as the skin of the oil sac.

Based on an initial actuator size, the parameter optimization experiment was carried out by varying the opening angle of the sector contour and the electrode size. Considering the high precision of laser processing, we can perform millimeter-level geometric parameter adjustments. For the opening angle of the sector contour α, we choose the middle range from 80 degrees to 120 degrees, and the opening angle is set to be 80 degrees, 90 degrees, 100 degrees, 110 degrees, and 120 degrees, with an increment of every 10 degrees, separately. For the electrode size, we choose to increase the radius R by 1 mm successively. At the same time, four new electrode shapes need to be customized to match the actuator geometry with different opening angle characteristics. Eight new electrode shapes need to be customized, four of which take an angle as the variable, and the rest take radius length as the variable (Fig. 2A).

We took electrode radius as the independent variable and longitudinal elongation as the dependent variable. Under different actuating voltages, the three curves showed a trend of first increasing and then decreasing; and reached the highest value of elongation when the electrode radius was 20 mm (Fig. 2B). Therefore, a radius of 20 mm may be close to the inflection point of HESA's strain performance. According to the calculation, when the electrode radius is 20 mm, the maximum longitudinal elongation is 128.7%. However, the 18 mm radius electrode only has an 83.4% elongation. Under the conditions of different electrode radii, the following experimental results can be obtained using 3 kV, 4 kV, and 5 kV as independent variables and longitudinal elongation as the dependent variable. For each electrode size, the increased applied voltage did not significantly change in longitudinal elongation (Fig. 2C). Therefore, it is more appropriate to choose a smaller voltage considering the energy consumption. Indeed, something still needs to be noted here is that, due to the characteristics of the actuator, it is necessary to ensure that the actuating voltage meets the activation voltage threshold. When actuated by different voltages, the longitudinal elongation of actuators with opening angles of 90° and 110° almost remained unchanged, while the longitudinal elongation of actuators with other opening angles increased with the increase of actuating voltage (Fig. 2D).

This data indicates that for the latter, the actuating voltage in the range of 3 kV to 5 kV is not enough to make the two electrodes fit closely, and the actuating efficiency needs to be improved. In subsequent experiments, the actuating voltage should be increased at equal intervals until the plot flattens out, indicating that the maximum actuating efficiency has been reached, and further increasing the actuating voltage will only waste energy. We took the opening angle as the independent variable and the longitudinal elongation as the dependent variable, and the relevant experimental results can be seen. It can be seen that, despite some fluctuations, there is an overall increasing trend. Based on the analysis of this result, this paper believes that the opening angle will change the oil distribution in the actuator unit. The larger the opening angle, the more uniform the corresponding distribution will be, and the smaller the distance gap between the farthest and nearest electrode plates will be, which means that the actuator is more likely to have a “zipping” effect [22] and better actuating performance.

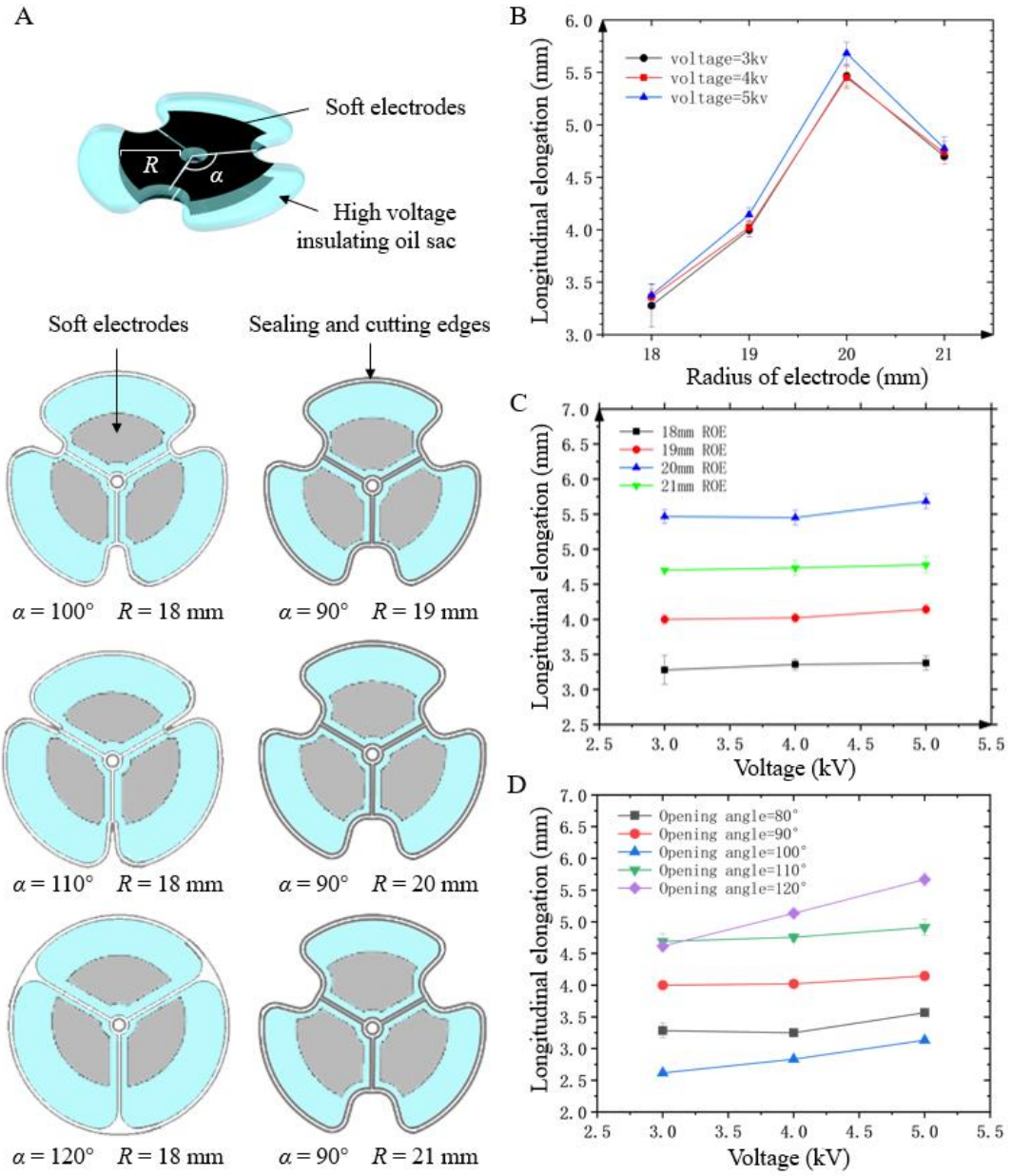

Fig. 1. The elongation performance of the HESA. (**A**) Design HESA with different dimensions by adjusting open angle α and soft electrodes radius R. (**B**) The influence of voltage input on the longitudinal elongation, including the radius of electrodes. (**C**) The influence of the radius of electrodes on the longitudinal elongation, including the actuation voltage. (**D**) The influence of voltage input on the longitudinal elongation, including the opening angle of the electrodes.

2.3 Using the laser to process HESA soft actuator

In order to produce HESA actuators in batches and in a standardized manner, we propose a scheme (Fig. 3) to use a laser cutting machine for skin processing. Laser cutting uses a focused high-frequency pulse and high-energy laser beam to interact with matter. High power density laser as energy source bombarding the membrane material,

material molecules absorb light energy and convert it into heat energy, rapidly heating local material. The TPU film material is a thermoplastic material that can melt at high temperatures. After cooling, the effect is similar to welding [23,24]. By setting different laser powers for different processing trajectories, the laser cutting machine can simultaneously heat seal (lower power) and cut (higher power) the oil sac skin.

Here, we use the heat generated by the laser to weld the membrane material. The use of laser welding has the following advantages: 1) The weld trace is narrow and has good potential for fine machining (the weld trace size is about 0.2 mm in the case of focus); 2) No contact force will be applied to membrane material during welding, resulting in no residual stress and consequent undesired deformation; 3) Various machining parameters and machining paths can be set to complete the heat sealing and cutting of the actuators at the same time in one run;4) The laser beam is maneuverable, which can realize the inertial-free emergency stop and fast steering; 5) Consistent with the conventional laser cutting method, no additional operation learning is required.

When processing with a laser cutting machine, the TPU film is first cut to the appropriate size and cleaned, then the two layers are stacked together, flattened, and fixed on the laser cutting working plane. Then focus the laser head by placing the matching focus tool on the membrane and adjusting the operating platform to the appropriate height. Then open the air pump of the laser operating platform, and use the airflow suction to fit the film on the processing platform. Finally, the file is imported, and the appropriate processing parameters are set in the processing settings to process the oil sac skin.

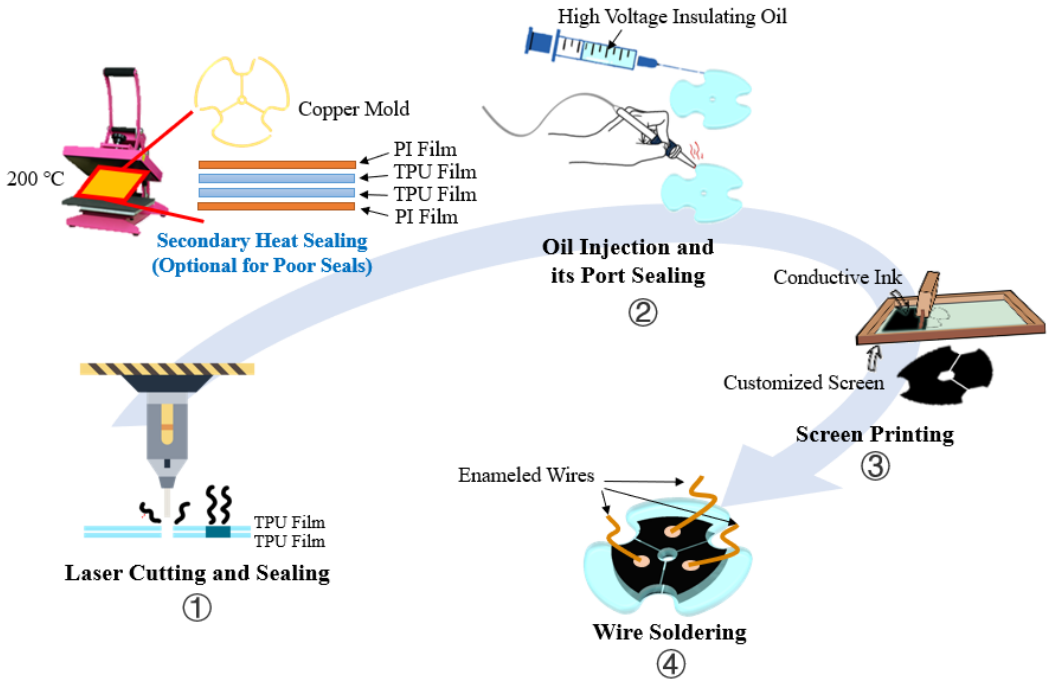

Fig. 2. The fabrication process of the HESA based on laser processing. Firstly, use a laser etching system to seal and cut the oil sac skin by adjusting the power of the laser.

If some skin has poor sealing, it is optional to use a hot press and the copper mold for secondary sealing. Secondly, add an appropriate amount of high-voltage insulating oil into the skin using a syringe. Thirdly, print electrodes on the prepared oil sac by screen printing. Fourthly, weld enameled wires to the small copper tape discs and stick them on the flexible electrodes.

The setting of laser parameters has a significant influence on fabrication. Power and speed affect thermal sealing. Too high power or too slow speed will lead to the burning through of the film, while too low power or too fast speed will lead to poor heat sealing (Fig. 4A). The pulse frequency of the laser also affects the density of heat-sealing points. The influence of laser parameters (power, speed, and pulses per inch (PPI)) on the processing effect will be analyzed in detail in the Results and Analysis chapter. In general, the influence of power and speed on the heat-sealing effect is roughly an inverted U-shaped curve: with the increase of power or speed, the heat-sealing result will get better and then get worse.

Another drawback of the heat seal is the bubbles produced by the material when heated, which can also easily cause seal failure (Fig. 4B). In addition, the cleanliness of the membrane surface (Fig. 4C) also has a great influence on the processing effect. The invisible dust and hair in the air will cause great damage to the effect of heat sealing. In practice, the two layers of the film do not require a high degree of close fit. A smaller uniform gap does not affect hot working because the processing platform's airflow suction and the laser's microkinetic energy can help the working point to fit well. However, if the space between two layers of the film is larger, or there is any fold on the film, it will also cause the consequence that the upper membrane has been cut off, but no sealing between the upper and lower membrane because the heat has not been transferred to the lower membrane sufficiently.

By adding a high-power processing route at the lateral of the model, it can directly cut off the sealed oil sac completely. The solution of using laser processing of oil sac skins allows simpler iterations of the geometry design; and the high volume, standardized production of oil sac without the worry that subsequent cutting will destroy the sealing performance of the oil sac. However, at the same time, laser processing also faces some challenges. The test of the parameters is needed for different sealing geometries because the interpolation algorithm of the positioning of the laser head movement speed is not the same between different types of paths. For example, the linear velocity is not the same in the same speed setting in a straight line and arc sealing. Therefore, adjusting different speeds and pulse numbers for the different paths is necessary to prevent some sections from being burned through before other sections are heat-sealed (Fig. 4D).

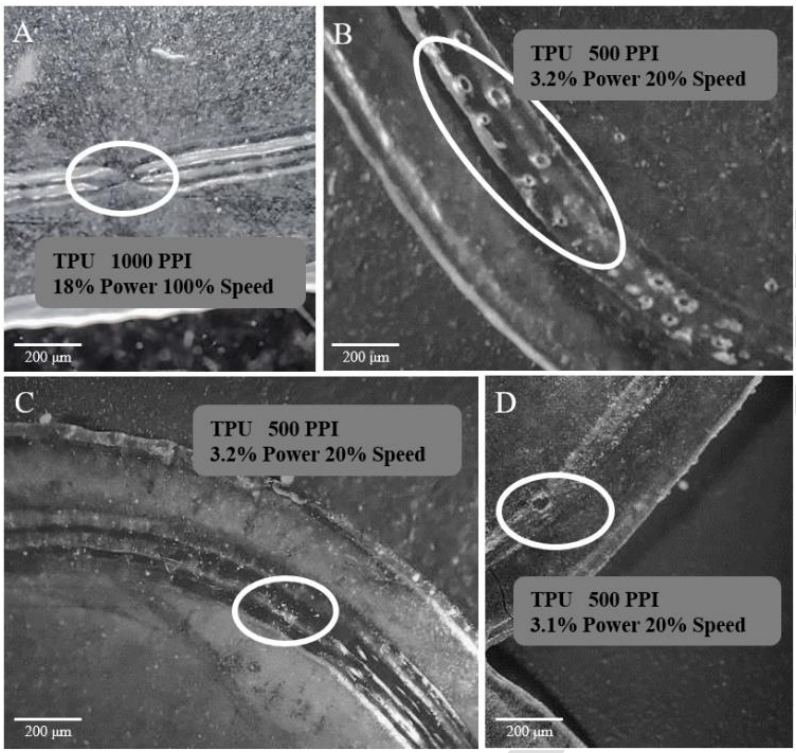

Fig. 3. Causes of failure under different fabrication parameters. (**A**) Heat sealing failure. (**B**) A large number of bubbles. (**C**) Unclean TPU surface. (**D**) Laser burn-through

2.4 Mathematical modeling and simulation of the actuator

The influence of geometric parameters on the actuator's performance can only be explored through repeated experiments in the above description. In order to reliably predict the performance of the actuator systematically, we established the outline of the geometric physical model of the actuator (Fig. 5A and Fig. 5B) according to the experimental results of the actuator and the abstract description of its shape change.

We assume that the oil of the actuator is wrapped by a fan-shaped cylindrical film, in which the radius of the sector is R_1 and the opening angle is α. The total internal oil quantity is V. Considering that the average radial shrinkage rate in the parametric experiment is less than 10%, the value of R_1 is assumed to remain unchanged. The radius of the flexible sector electrode is R_2, and the distance between the upper and lower plates is evenly distributed. In this case, the thickness of the film is h_0. When high voltage U is applied to the electrode, the plate spacing g decreases, the volume on the right side of the oil sac increases, and the film thickness becomes h_1. Ideally, we assume that oil is incompressible. The following figure shows how the parameters are changed and the effect before and after deformation.

We assume that the film does not deform in the initial state; that is, there is no pressure between the film and the oil, so the initial pressure $P_{in} = 0$. After applying high voltage, the electrode plate attracts each other under the electrostatic pressure. The oil is squeezed to the outside of the film so that the film is forced and deformed. Furthermore, the internal pressure increases at the same time. As each electrode plate continues to be subjected to electrostatic pressure, the distance decreases, and the internal pressure increases continuously until the system reaches dynamic equilibrium.

The following equation can calculate the deformations in the above process. First, the volume expressions before and after the deformation can be coupled with the iso-volume property of the oil:

$$V = \frac{\alpha\pi {R_2}^2 g}{360} + \frac{\alpha h_1 \pi (R_1 - R_2) \times \frac{1}{2}(R_1 + R_2)}{360} \tag{1}$$

We can get film thickness h_1:

$$h_1 = \frac{\frac{360}{2\pi}V - {R_2}^2 g}{{R_1}^2 - {R_2}^2} \tag{2}$$

We use the equation for the shear elastic deformation of TPU films to relate the pressure and the change of area:

$$E_{shear} = \frac{F/A}{\Delta A/A} \tag{3}$$

In which

$$\Delta A = A_{after} - A_{before} \tag{4}$$

$$A_{before} = \frac{\alpha}{360} \times 2\pi \times \left({R_1}^2 - {R_2}^2\right) + h_0 \times [\frac{\alpha}{360} \times 2\pi R_1 + 2(R_1 + R_2)] \quad (5)$$

$$A_{after} = (2h_1 - g)\frac{\alpha}{360} \times 2\pi R_2 + 2(R_1 - R_2)\mathrm{b} + \frac{\alpha}{360} \times 2\pi \times \left({R_1}^2 - {R_2}^2\right) \quad (6)$$

So the internal pressure can be calculated as follows:

$$P_{in} = \frac{F}{A} = E\frac{\Delta A}{A} \quad (7)$$

According to the formula of electrostatic pressure of flexible electrodes in Edouard Leroy's paper [25]:

$$P_{elec} = \frac{\varepsilon_0 \varepsilon_{eq} U^2}{2(t_{dielectric} + g)^2} \quad (8)$$

Where U is the voltage, g is the distance between the top membrane and the bottom substrate and $t_{dielectric}$ is the dielectric thickness. ε_{eq} is an equivalent dielectric constant taking into account the fluid thickness and permittivity:

$$\varepsilon_{eq} = \frac{\varepsilon_{dielectric} t_{dielectric} + \varepsilon_{fluid} g}{t_{dielectric} + g} \quad (9)$$

Where $\varepsilon_{dielectric}$ and ε_{fluid} are the relative permittivity of the dielectric material and the fluid. For all models we presented here, $\varepsilon_{dielectric} = 40$, $\varepsilon_{fluid} = 3$ and $t_{dielectric} = 20\ \mu m$.

Finally, we can calculate the parameters g, h_1, P_{in} when the HESA reaches a steady state by combining the equation for the internal pressure and the electrode pressure.

$$P_{elec} = \frac{F}{A} = E\frac{\Delta A}{A} = P_{in} \quad (10)$$

We can solve for g and h_1 for different parameters by combining the above equations with numerical approximation. As a result, we could simulate the longitudinal elongation and the gap of the electrodes. Taking HESA with parameters R_2 is 18 mm, V is 1.5 ml, and α is 90° as an example, we have made the following three figures through the above model, which correspond to the experimental elongation results. The actuator elongation increases with the increase of electrode radius. When R_2 is between 22 mm and 23 mm, it reaches a peak value (Fig. 5C). This result is within a reasonable range compared with the value of 20 mm in the actual experiment. The effect of voltage reduction on elongation also shows a trend of increasing from fast to slow, which is consistent with the theory of saturation voltage mentioned above. When the voltage is greater than 15 kV, the growth rate of longitudinal elongation decreases significantly as the increase of voltage (Fig. 5D). Similarly, from the perspective of the variation of the electrode gap with the applied voltage, it is more and more challenging to reduce the electrode spacing when it is greater than 10 kV (Fig. 5E). Therefore, in future design, an appropriate actuating voltage should be selected from the perspective of energy conversion efficiency.

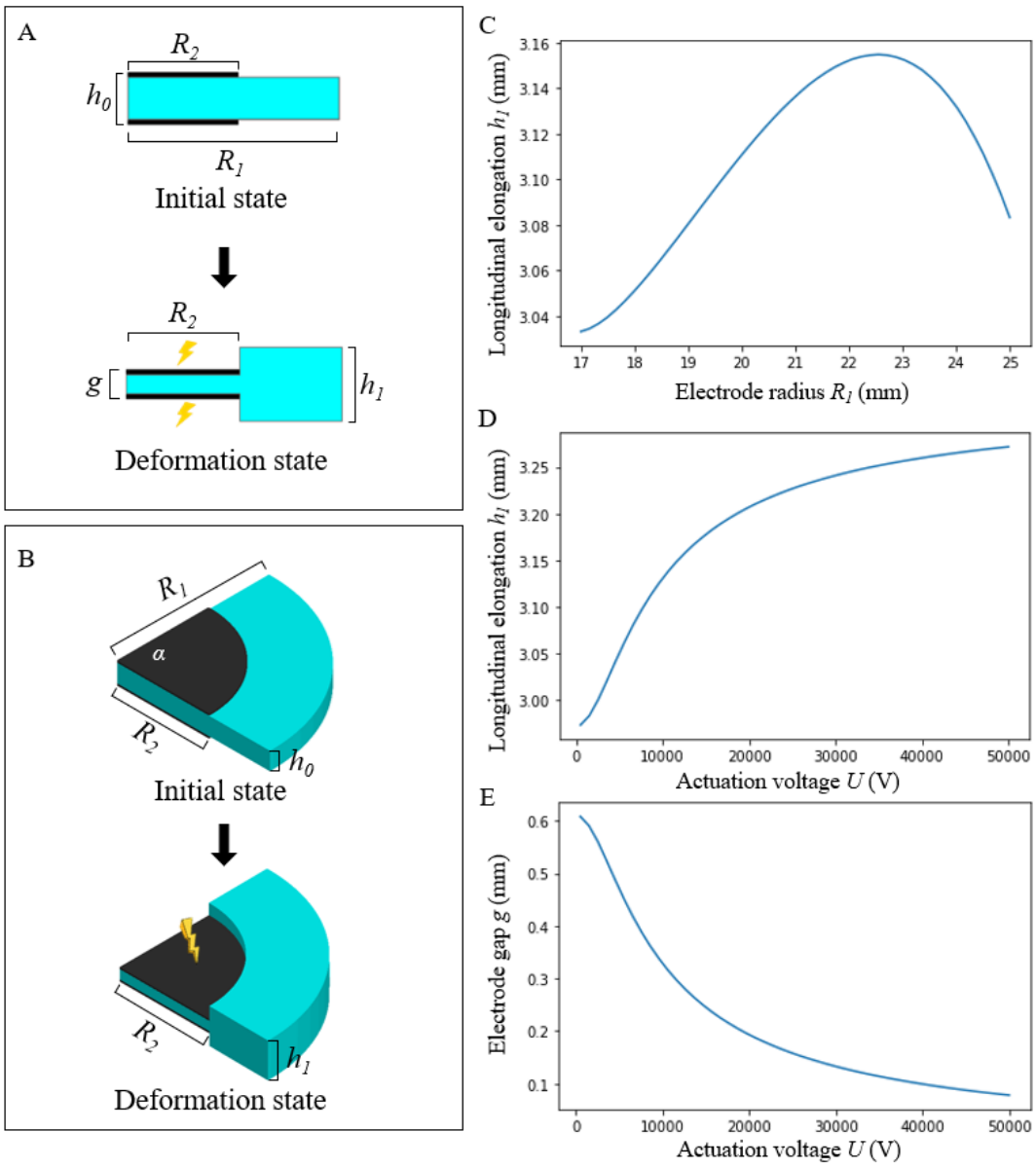

Fig. 4. Single channel modeling of the HESA. (**A**) Section view. (**B**) Axonometric view. (**B**) The influence of the electrode radius on the longitudinal expansion. (**C**) The influence of the actuation voltage on the longitudinal expansion. (**D**) The influence of the actuation voltage on the gap between a pair of soft electrodes.

3. Results and analysis

After implementing the manufacturing process of HESA with a new method, the relationship between the machining effect and laser parameters in laser processing is studied deeply. In addition, we also carried out experiments to explore the motion performance of the single piece and multi pieces of actuators. Real-time capacitance

sensing data acquisition is also attempted for each actuator channel.

3.1 Influence of laser processing parameter setting on machining effect

Different laser processing parameters have a significant influence on welding. In the actual processing process, we control and adjust the laser parameters to experiment with the morphology change of the weld trace under single factor variables, including power, laser moving speed, laser pulse number, and defocus. A study of the weld trace through a 20x optical magnification reveals that the sealing will fail with too fast speed or too low power. Under the above situation, the processed film cannot receive enough energy to heat up to the required sealing temperature. On the contrary, too slow speed or too high power will absorb excess energy and cause a high temperature to cut off the film.

High speed and high power will make laser sealing unevenly on the film, leading to a discontinuous weld trace. The welding trace at the first part of the processing absorbs more energy, so the welding trace is wider than desired. And the later part of the processing, the welding trace gradually becomes less visible. If the power continues to increase, discontinuous comet-like burning holes will appear (Fig. 6A). In addition, it is possible to produce bubbles in the weld under any machining parameters. According to the current experiments, this does not affect the welding strength and sealing effect. Based on the results of several experiments, we can make the following summary: too high power and too slow speed will lead to burn through, too low power and too fast speed will lead to welding failure, and PPI affects the uniformity of welding.

We comprehensively scored the weld strength obtained by manual pull failure, the machining defects observed by microscope, and the sealing effect obtained by the oil injection test. We plotted the distribution of welding defects and the welding effect score in the graph with the moving speed of the laser head and laser power as the horizontal and vertical coordinates to obtain the following chart (Fig. 6B). The main defect forms under this machining parameter are classified by color, and the numbers indicate the welding effect. The higher the score value is, the better the damage tolerance and sealing performance are, and the fewer the machining defects are. Experiments show that some defects observed by microscope have no causal relationship with welding strength and sealing performance, such as a small number of bubbles in the weld or a small number of burning holes having little effect on sealing performance.

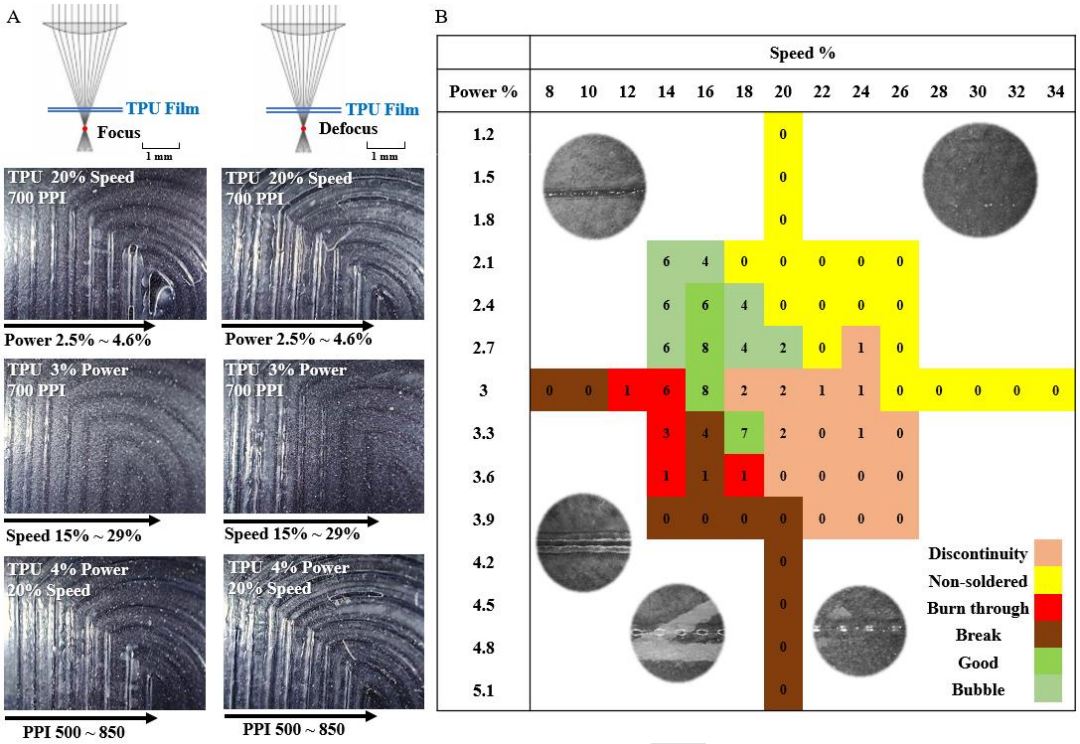

Fig. 5. Welding results due to different processing parameters. (**A**) Welding traces through different laser speeds, power, and PPI. (**B**) Defect distribution and evaluation of welding results.

3.1 Movements of single HESA actuator

The electrodes are printed on the oil sac of the soft actuator by screen printing and connected to the driver board by copper tape and enameled wire. At an excitation voltage of 5 kV, the soft actuator provides greater strain and faster response. We measured the deformation of the actuator using a grid plate (Fig. 7). A single soft actuator, driven by a voltage of 5 V, can simultaneously realize shrinkage in the radius direction and elongation along the axis direction. The strain in the radius direction can reach 7.8%, and the strain along the axis direction can reach 32.2%.

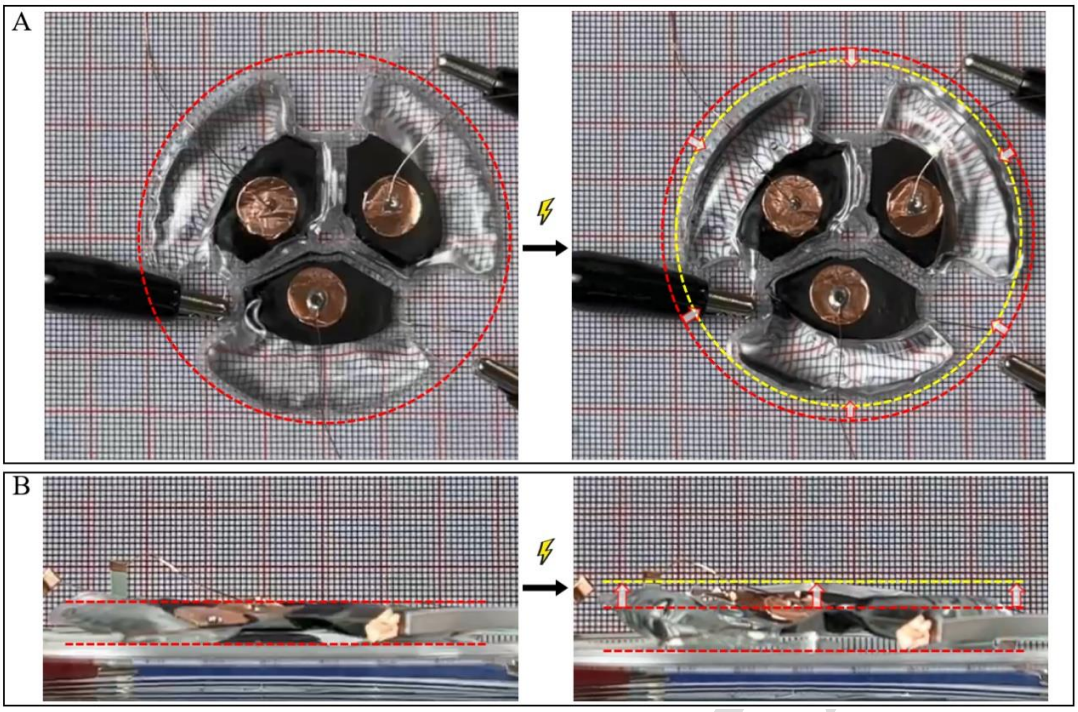

Fig. 6. The actuation of the single piece of the HESA. (**A**) The top view shows 7.8% radius shrinkage. (**B**) The front view shows 32.2% axial elongation.

3.2 Movements of stacked HESA actuators

The transverse musculature of the octopus muscle is not a thin layer, so we stacked three actuators on top of each other and activated them at 5 kV. We first connected all channels of the HESA in parallel with 5 kV voltage. When energized, the three pairs of flexible electrodes in the three channels attract each other, forcing dielectric oil into the three cavities, which causes the entire actuator elongates accordingly (Fig. 8A). According to the same principle, frequencies of 1 Hz, 5 Hz, and 10 Hz were used for actuation. The elongation length curve with time was obtained (Fig. 8B to Fig. 8D). Overall, the actuator elongation decreases with increasing frequency. The elongation range was shifting slightly at 5 Hz actuation (Fig. 8C). Then, to test the bending ability of the biomimetic octopus transverse musculature, we electrically actuated two of these channels. As the actuated two cavities expand and only one cavity remains the same shape, the actuator produces a bending motion (Fig. 8E). Based on the same principle, frequencies of 1 Hz, 5 Hz, and 10 Hz were applied for actuation, and the curve in Fig. 8F to Fig. 8H was obtained. We can see that the actuation works fairly steadily. The range of motion at 1 Hz is the largest, while the range of motion at 5 Hz and 10 Hz is relatively consistent. Interestingly, the actuator exhibits two fixed cycle posture recovery positions during the bending motion at 10 Hz.

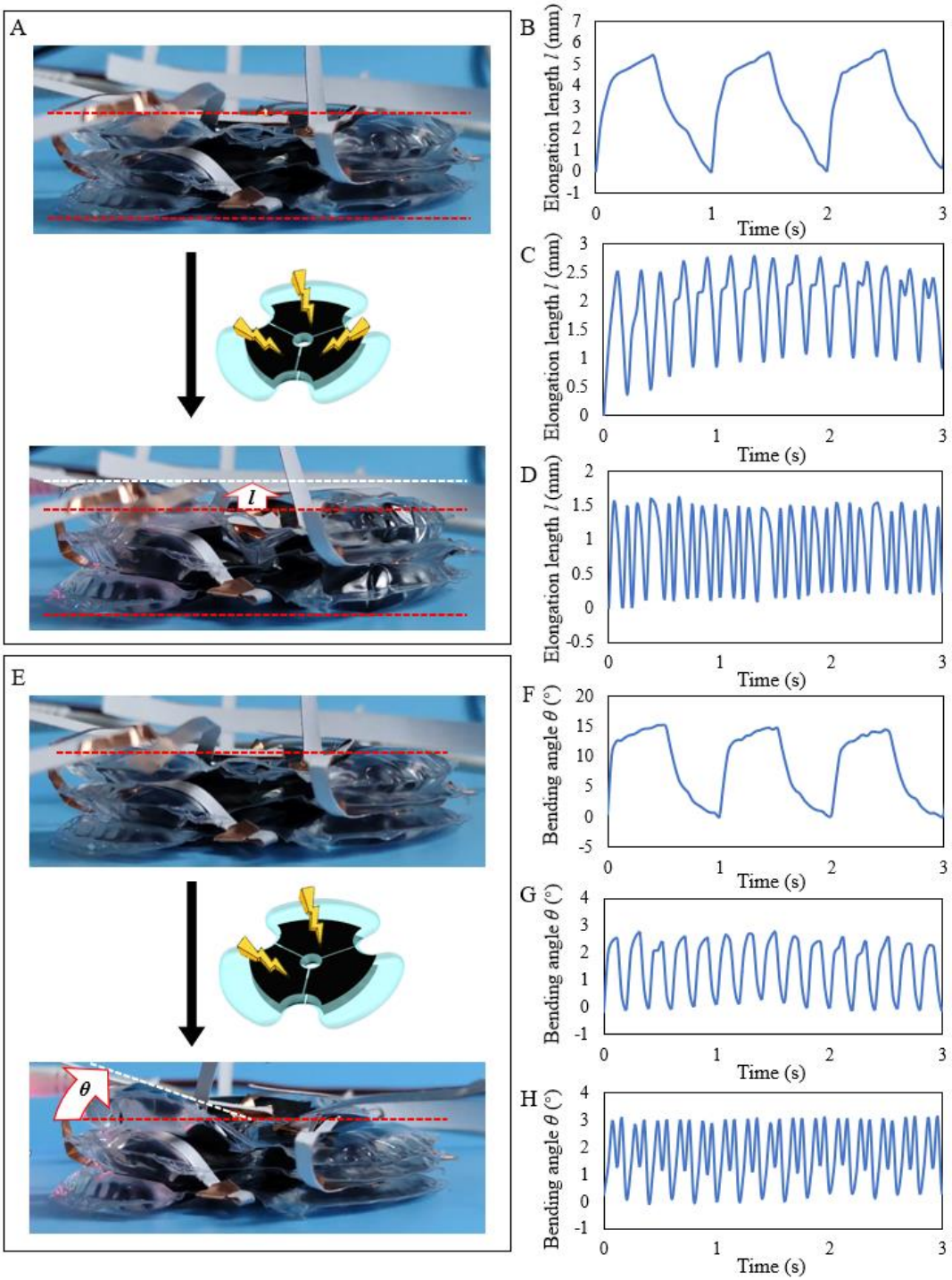

Fig. 7. The actuation at 5 kV of a stack of HESA pieces. (**A**) *l* mm elongation through the actuation of three channels of the HESA pieces. (**B**) Elongation length with time at an actuation of 1 Hz. (**C**) Elongation length with time at an actuation of 5 Hz. (**D**) Elongation length with time at an actuation of 10 Hz (**E**) *θ* degree bending through the actuation of two channels. (**F**) Bending angle with time at an actuation of 1 Hz. (**G**) Bending angle with time at an actuation of 5 Hz. (**H**) Bending angle with time at an actuation of 10 Hz.

4. Discussion and conclusion

This paper designed a hydrostatic electroactive soft actuator inspired by the transverse musculature of octopus. We explored the application of a typical laser cutting machine to seal and cut the actuator's oil sac in one run, which is more convenient than the current fabrication methods of HASEL actuators [17–21].

We did laser processing experiments to evaluate the strength of the welding. The influence of different parameters on the welding effect was discussed. In general, within a specific range, under the same power, with the increase of laser moving speed, the welding result first increases and then decreases; at the same moving speed, the welding result increases with the increase of laser power first and then decreases.

The maximum longitudinal elongation values under different geometry parameters were tested by changing the element's opening angle, the flexible electrode's radius, and the actuation voltage. The elongation curves relative to electrode shape and voltage were obtained, and the relationship and trend of these curves were discussed. We also modeled the geometric shape of one channel of the HESA mathematically. Furthermore, through the mathematical model simulation, we obtained the optimal size parameters close to the experiment results.

Based on well-behaved design parameters, we performed measurements of the single piece of HESA actuator. We verified that the actuator achieves contraction in the radius direction while having a large axial elongation, similar to the octopus's transverse musculature movement. In addition, we placed three actuators on top of each other, and by applying a voltage to either two or three channels, we showed the elongation and bending motions of a stack of actuators at different frequencies. The motion modes of the octopus transverse musculature are achieved. In the future, the benefit of the constant volume actuation of the transverse musculature will be explored based on this kind of actuator.

Declaration of competing interest

The authors declare that they have no known competing financial interests or personal relationships that could have appeared to influence the work reported in this paper.

Acknowledgments

We would like to express our sincere thanks to Prof. Cecilia Laschi for their guidance and instruction and her help in this work. This work was supported by the National Natural Science Foundation support projects, China (Grant Nos. 92048302, 91848206, T2121003), and the National Key R&D Program of China (Grant Nos. 2019YFB1309600, 2020YFB1313003).

References

[1] G. Sumbre, Y. Gutfreund, G. Fiorito, T. Flash, B. Hochner, Control of Octopus Arm Extension by a Peripheral Motor Program, Science. 293 (2001) 1845–1848.

[2] Y. Gutfreund, T. Flash, G. Fiorito, B. Hochner, Patterns of Arm Muscle Activation Involved in Octopus Reaching Movements, J. Neurosci. 18 (1998) 5976–5987.

[3] E. Ramey, R. Ramey, L. Brown, S. Kelley, Desert-dwelling African elephants (Loxodonta africana) in Namibia dig wells to purify drinking water, Pachyderm. 53 (2013) 66–72.

[4] K. Autumn, Y.A. Liang, S.T. Hsieh, W. Zesch, W.P. Chan, T.W. Kenny, R. Fearing, R.J. Full, Adhesive force of a single gecko foot-hair, Nature. 405 (2000) 681–685.

[5] C. Laschi, M. Cianchetti, B. Mazzolai, L. Margheri, M. Follador, P. Dario, Soft Robot Arm Inspired by the Octopus, Advanced Robotics. 26 (2012) 709–727.

[6] Z. Xie, A.G. Domel, N. An, C. Green, Z. Gong, T. Wang, E.M. Knubben, J.C. Weaver, K. Bertoldi, L. Wen, Octopus Arm-Inspired Tapered Soft Actuators with Suckers for Improved Grasping, Soft Robotics. 7 (2020) 639–648.

[7] J. Fras, Y. Noh, M. Macias, H. Wurdemann, K. Althoefer, Bio-Inspired Octopus Robot Based on Novel Soft Fluidic Actuator, in: 2018 IEEE International Conference on Robotics and Automation (ICRA), IEEE, Brisbane, QLD, 2018: pp. 1583–1588.

[8] S. Zhuo, Z. Zhao, Z. Xie, Y. Hao, Y. Xu, T. Zhao, H. Li, E.M. Knubben, L. Wen, L. Jiang, M. Liu, Complex multiphase organohydrogels with programmable mechanics toward adaptive soft-matter machines, Sci. Adv. 6 (2020) eaax1464.

[9] S. Furukawa, S. Wakimoto, T. Kanda, H. Hagihara, A Soft Master-Slave Robot Mimicking Octopus Arm Structure Using Thin Artificial Muscles and Wire Encoders, Actuators. 8 (2019) 40.

[10] M. Cianchetti, A. Licofonte, M. Follador, F. Rogai, C. Laschi, Bioinspired Soft Actuation System Using Shape Memory Alloys, Actuators. 3 (2014) 226–244.

[11] M. Cianchetti, A. Arienti, M. Follador, B. Mazzolai, P. Dario, C. Laschi, Design concept and validation of a robotic arm inspired by the octopus, Materials Science and Engineering: C. 31 (2011) 1230–1239.

[12] M. Calisti, A. Arienti, M. Elena Giannaccini, M. Follador, M. Giorelli, M. Cianchetti, B. Mazzolai, C. Laschi, P. Dario, Study and fabrication of bioinspired Octopus arm mockups tested on a multipurpose platform, in: 2010 3rd IEEE RAS & EMBS International Conference on Biomedical Robotics and Biomechatronics, IEEE, Tokyo, Japan, 2010: pp. 461–466.

[13] C. Laschi, B. Mazzolai, V. Mattoli, M. Cianchetti, P. Dario, Design of a biomimetic robotic octopus arm, Bioinspir. Biomim. 4 (2009) 015006.

[14] T. Doi, S. Wakimoto, K. Suzumori, K. Mori, Proposal of flexible robotic arm with thin McKibben actuators mimicking octopus arm structure, in: 2016 IEEE/RSJ International Conference on Intelligent Robots and Systems (IROS), IEEE, Daejeon, South Korea, 2016: pp. 5503–5508.

[15] W.M. Kier, M.P. Stella, The arrangement and function of octopus arm musculature and connective tissue, J. Morphol. 268 (2007) 831–843.

[16] F. Carpi, S. Bauer, D. De Rossi, Stretching Dielectric Elastomer Performance, Science. 330 (2010) 1759–1761.

[17] E. Acome, S.K. Mitchell, T.G. Morrissey, M.B. Emmett, C. Benjamin, M. King, M. Radakovitz, C. Keplinger, Hydraulically amplified self-healing electrostatic actuators with muscle-like performance, Science. 359 (2018) 61–65.

[18] R. Chen, Z. Yuan, J. Guo, L. Bai, X. Zhu, F. Liu, H. Pu, L. Xin, Y. Peng, J. Luo, L. Wen, Y. Sun, Legless soft robots capable of rapid, continuous, and steered jumping, Nat Commun. 12 (2021) 7028.

[19] N. Kellaris, V. Gopaluni Venkata, G.M. Smith, S.K. Mitchell, C. Keplinger, Peano-HASEL actuators: Muscle-mimetic, electrohydraulic transducers that linearly contract on activation, Sci. Robot. 3 (2018) eaar3276.

[20] S.K. Mitchell, X. Wang, E. Acome, T. Martin, K. Ly, N. Kellaris, V.G. Venkata, C. Keplinger, An Easy- to- Implement Toolkit to Create Versatile and High-Performance HASEL Actuators for Untethered Soft Robots, Adv. Sci. 6 (2019)

[21] X. Wang, S.K. Mitchell, E.H. Rumley, P. Rothemund, C. Keplinger, High- Strain Peano- HASEL Actuators, Adv. Funct. Mater. 30 (2020) 1908821.

[22] R.S. Diteesawat, T. Helps, M. Taghavi, J. Rossiter, Electro-pneumatic pumps for soft robotics, Sci. Robot. 6 (2021) eabc3721.

[23] A.A. Amiri Moghadam, S. Alaie, S. Deb Nath, M. Aghasizade Shaarbaf, J.K. Min, S. Dunham, B. Mosadegh, Laser Cutting as a Rapid Method for Fabricating Thin Soft Pneumatic Actuators and Robots, Soft Robotics. 5 (2018) 443–451.

[24] D. Zhang, X. Wang, M. Tian, D. Shen, Y. Mao, A Novel Manufacturing Method for Thermoplastic Polyurethane Welding Using CO2 Laser, in: 2019 IEEE International Conference on Mechatronics and Automation (ICMA), IEEE, Tianjin, China, 2019: pp. 1687–1691.

[25] E. Leroy, R. Hinchet, H. Shea, Multimode Hydraulically Amplified Electrostatic Actuators for Wearable Haptics, Adv. Mater. (2020) 2002564.

Declaration of interests

☒ The authors declare that they have no known competing financial interests or personal relationships that could have appeared to influence the work reported in this paper.

☐The authors declare the following financial interests/personal relationships which may be considered as potential competing interests: